



**SHocks:
structure, AcceleRation, dissiPation**

Work Package 5

Database of shock crossings and software
repository

Deliverable D5.4

Technical report on the complete developed shock
database

N. Ganushkina, M. Gedalin, M. van de Kamp,
and SHARP Team

31/12/2023

This project has received funding from the European Union's Horizon 2020
research and innovation programme under grant agreement No 101004131



Document Change Record

Issue	Date	Author	Details
V1.0	December 16, 2023	N. Ganushkina	Sent to main co-authors for comments
V2.0	December 24, 2023	N. Ganushkina	Sent to SHARP team for comments
V2.0	December 30, 2023	N. Ganushkina	Uploaded to EU Portal

Table of Contents

1	Summary	3
2	Introduction	3
3	SHARP database: General structure and access	4
4	Spacecraft data used for database development and calculations of shock parameters	6
4.1	Terrestrial shocks	9
4.2	Interplanetary shocks	10
4.3	Shocks at non-magnetized planets	12
5	References	16

1 Summary

Deliverable D5.4 entitled "Technical report on the complete developed shock database" is the final deliverable of WP5 entitled "Database of shock crossings and software repository". The Objectives of WP5 were (1) to generate a database of shock crossings observed by terrestrial and planetary missions, and (2) to freely disseminate the shock database and analysis tools to the community. The Deliverable D5.4 presents the newly-developed SHARP shock database built using the measurements from Cluster, MMS, THEMIS/ARTEMIS, MAVEN and VEX missions. The SHARP shock database can be accessed via SHARP project website at <https://sharp.fmi.fi/shock-database/>. The developed database allows large-scale comparisons of collisionless shocks across a vast array of parameters.

2 Introduction

Collisionless shocks (CSs) are one of the most fundamental phenomena in space and one of the most powerful accelerators in the Universe. Collisionless Shocks are found in almost every plasma environment observed either directly or indirectly such as: the Earth's bow shock that forms the interface between the solar wind and the terrestrial magnetosphere, bow shocks in the vicinity of other planets, interplanetary shocks that separate different flows within the solar wind, at the boundaries of solar systems or heliospheres, around other stars, supernovae remnants, gamma-ray bursts, active galactic nuclei, and cluster of galaxies. CSs exist at all scales in the Universe: from only one centimetre in laboratory plasmas to megaparsec scales in galaxy clusters.

CSs are, in many aspects, a unique plasma phenomenon. They are the most effective energizers of charged particles capable of accelerating particles to very high energies (even up to $\sim 10^{20}$ eV). CSs are multi-scale objects where the interaction between the electromagnetic fields and charged particles provide the dissipation across all scales, starting with the electron inertial scale within the shock transition layer, and ending with the overall scale of the physical system. Physical processes at all these scales are interrelated. CSs are strongly nonlinear objects where the field-particle interactions are crucial. Understanding physics of CSs is not only necessary for knowledge of their outstanding role in the activity of most of the known objects in the universe. This is also relevant to the most fundamental phenomena in space plasmas such as acceleration, multi-scale processes, dissipation, and transition to irreversibility.

Despite more than half a century of collisionless shock research, our understanding of the processes of the shock energy dissipation into the charge particle heating and acceleration remains incomplete. The only available laboratory where CSs can be studied with in situ measurements is the heliosphere. However, very often the rate of the data analysis is well below of the rate of the data acquisition. Several attempts to develop shock databases have been made using various satellite data. The University of Helsinki's Heliospheric Shock Database (www.ipshocks.fi/) is built for Interplanetary shocks on the measurements from several spacecraft, covering time intervals from the 1970s (Helios A and B) to 2018 (Wind, ACE (Advanced Composition Explorer), Cluster and Stereo (Solar TERrestrial RELations Observatory) A and B) and provides the shock crossing

times, shock geometry and shock dynamics parameters and Alfvénic Mach number (M_A). A database on terrestrial bow shock crossings can be found at Cluster Science Archive (<https://www.cosmos.esa.int/web/csa/bow-shock-magnetopause-crossings>) which contains 529 events observed by Cluster spacecraft between years 2001 and 2013 Kruparova et al. [2019]. Meanwhile, a centralised shock database with the relevant advanced tools for the efficient exploitation of data is missing.

The main objective of the SHARP project was to achieve a major leap in the understanding of the structure of collisionless shocks in various environments and of the acceleration processes at all shock scales. One of the goals was to develop an open-source high-level database of shocks and a centralised source of advanced tools for the purpose of analysing shock structure and dynamics. The Deliverable D5.4 presents the newly-developed SHARP shock database built with general structure described using the measurements from Cluster, MMS, THEMIS (Time History of Events and Macroscale Interactions during Substorms)/ARTEMIS (Acceleration, Reconnection, Turbulence and Electrodynamics of the Moon's Interaction with the Sun), MAVEN (Mars Atmosphere and Volatile Evolution) and VEX (Venus Express) missions.

3 SHARP database: General structure and access

The SHARP database can be accessed via <https://sharp.fmi.fi/shock-database/>. Figure 1 demonstrates the possibilities for building of outputs from the SHARP shock database. First option for a user is to download the entire database of shocks in as an XML or CSV files or/and to download the plots of all shocks available in the database as TAR archive file. This option does not require selection of specific satellite data or any shock parameters.

The second option is to build a user-defined shock database. To see a list of all available data (6112 shocks), a user can simply click on Submit button. To create any specific output from the SHARP shock database, a user can select spacecraft mission/missions and/or adjust any parameter range, before clicking 'Submit'. The following missions can be selected: MMS for terrestrial bow shocks, MAVEN for Martian bow shocks, VEX for Venusian bow shocks, THEMIS B and C ('Artemis' since 2010) for interplanetary shocks, and CLUSTER for terrestrial bow shocks. Note that if none of the specific satellites is selected, the data from all of them will be included.

Figure 2 presents the list of the shock parameters included in the SHARP shock database with pre-defined ranges. The details on the shock parameters and their calculations are given in Section 4. If 'Include shocks without ... value' for a certain parameter is unchecked, shocks where the corresponding parameter value is unavailable will not be included. It is not recommended to use the 'back' and 'forward' buttons on the browser, as the website may not work properly while using them.

Figure 3 shows the output from the SHARP shock database when when no specific spacecraft is selected and no parameter is adjusted. The output include all available data MMS, MAVEN, VEX, THEMIS, and CLUSTER satellites in both inbound and outbound directions. The selection can be modified at this step

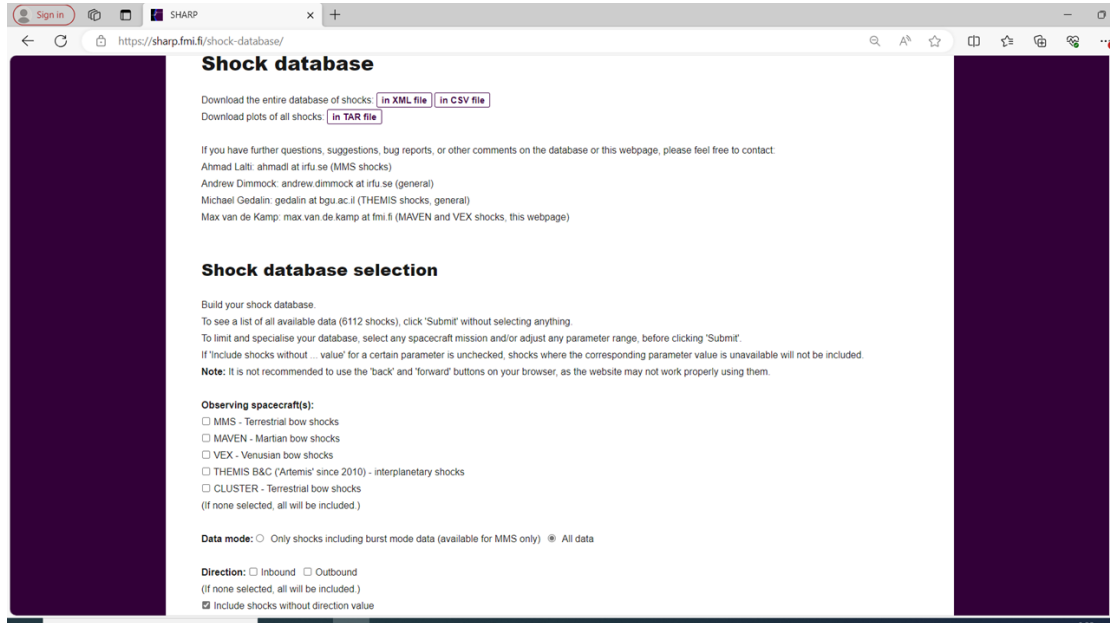


Figure 1: Options for building of outputs from the SHARP shock database at <https://sharp.fmi.fi/shock-database/>.

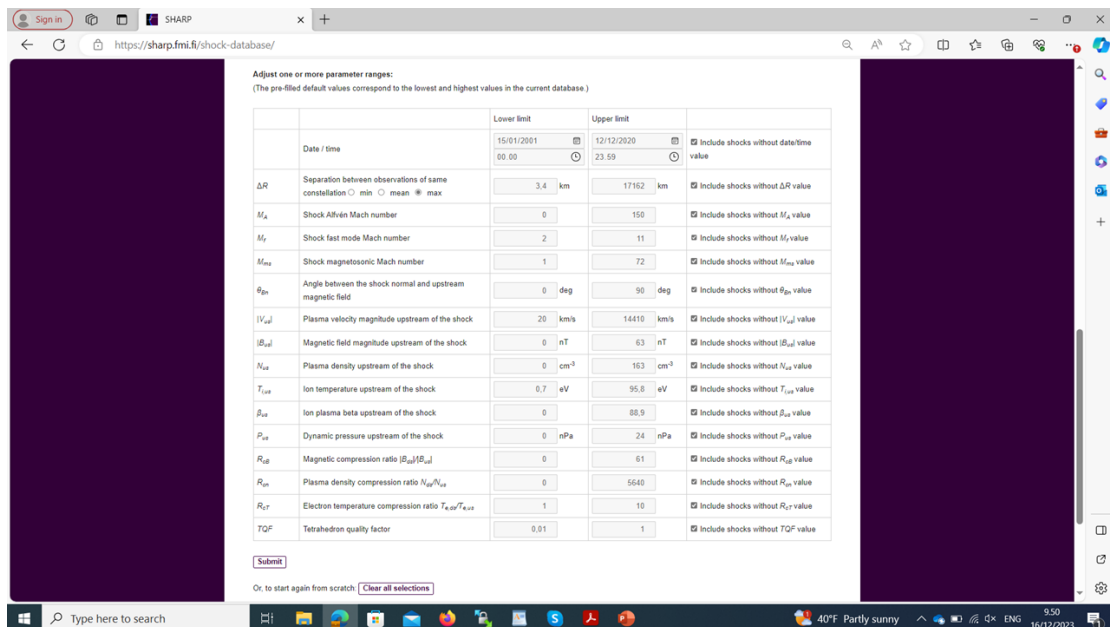


Figure 2: Shock parameters which ranges can be chosen (pre-defined values for ranges shown) included in the SHARP shock database.

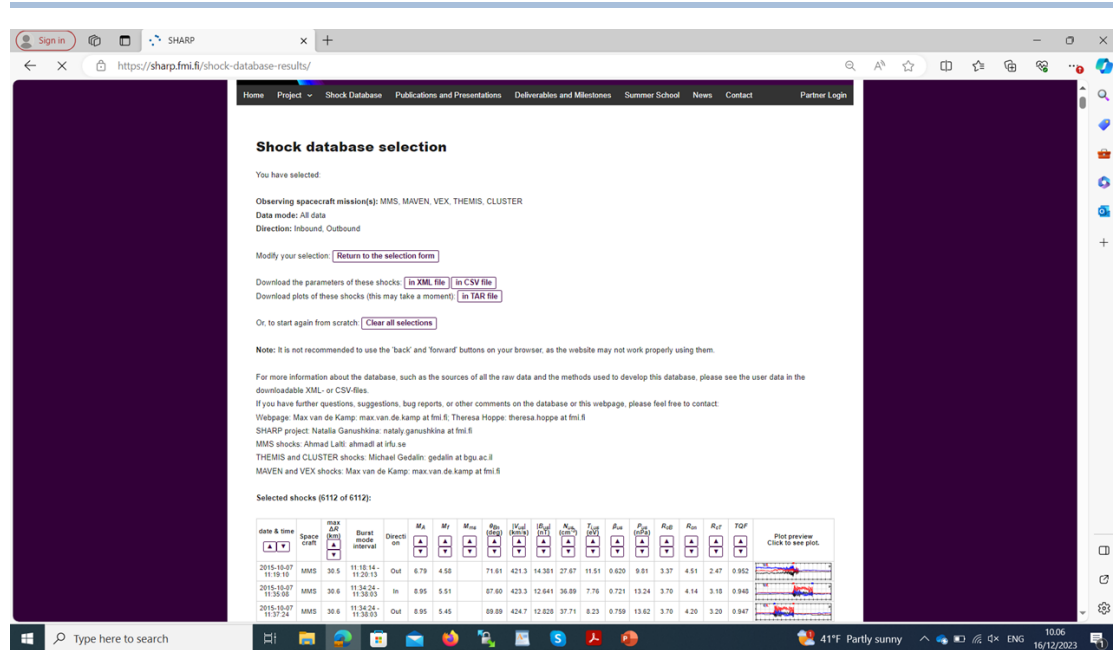


Figure 3: SHARP shock database output when no specific spacecraft is selected and no parameter is adjusted.

by clicking on the Return to the selection form button. The shock parameters for this selection can be downloaded in the XML and CSV file formats, whereas the shock plots can be downloaded in the TAR archive file format. The downloadable XML and CSV files contain the user data about the database, such as the sources of all the raw data and the methods used to develop the database. To start again from scratch, a user needs to click on Clear all selections button.

The output from the SHARP shock database is shown as a table (seen in the bottom of Figure 3 which contains date and time, spacecraft name, and all the available shock parameters with burst mode interval (MMS only) and direction (In and Out). The full name of the parameter appears when the cursor arrow is moved to the parameter’s symbol in the table. The last column in the table is the plot of corresponding data used to determine the shock parameters for that particular shock. Clicking on it will allow to see the full plot.

4 Spacecraft data used for database development and calculations of shock parameters

The SHARP shock database contains information about terrestrial shocks, interplanetary shocks and shocks at non-magnetized planets (Venus and Mars). The shock parameters which can be obtained depend on the available measurements in corresponding regions. The database contains the parameters which ranges can be chosen and the parameters which are pre-determined. Below is the list of shock parameters with adjustable ranges (Figure 2):

- Date [day.month.year] / Time UT [hours. minutes]: interval for shock measurements to output;

- ΔR [km]: Separation distance between observations of same constellation of satellites. Either the minimum, maximum or mean of all separations can be selected.
- M_A : Shock Alfvén Mach number;
- M_f : Shock fast mode Mach number;
- M_{ms} : Shock magnetosonic Mach number;
- θ_{Bn} [deg]: Angle between the shock normal \mathbf{n} and upstream magnetic field \mathbf{B}_{us} ;
- $|V_{us}|$ [km/s]: Plasma velocity magnitude upstream of the shock;
- $|B_{us}|$ [nT]: Magnetic field magnitude upstream of the shock;
- N_{us} [cm⁻³]: Plasma density upstream of the shock;
- $T_{i,us}$ [eV]: Ion temperature upstream of the shock;
- β_{us} : Ion plasma beta upstream of the shock;
- P_{us} [nPa]: Dynamic pressure upstream of the shock;
- R_{cB} : Magnetic compression ratio $|B_{ds}|/|B_{us}|$;
- R_{cn} : Plasma density compression ratio N_{ds}/N_{us} ;
- R_{cT} : Electron temperature compression ratio $T_{e,ds}/T_{e,us}$

The SHARP shock database output files also contain other parameters which depend on the satellite data used. Not all parameters can always be computed, for example, if the spacecraft separation is inappropriate (e.g. shock speed). In these cases, the parameter(s) will be flagged. Some parameters are never available for some of the missions.

The SHARP shock database output file contains the following parameters, in addition to the parameters which ranges can be chosen:

- direction (a flag indicating if the shock is inbound (1) or outbound (-1));
- $burst_{start}$ and $burst_{end}$ for the burst mode interval in epoch time (MMS data only);
- components B_{xus} , B_{yus} and B_{zus} [nT] of magnetic field upstream of the shock;
- standard deviation on the magnitude of the upstream magnetic field;
- $\Delta\theta_B$, the maximum rotation of the upstream magnetic field vector in the OMNI interval used;
- components V_{xus} , V_{yus} and V_{zus} [km/s] of the plasma velocity upstream of the shock;

Table 1: Availability of the SHARP shock database parameters.

Parameter/Mission	CLUSTER	MMS	THEMIS	MAVEN	VEX
Time	✓	✓	✓	✓	✓
Direction	✓	✓	✓	✓	✓
Burst interval		✓			
\mathbf{B}_{us}	✓	✓	✓	✓	✓
$\sigma(B_{us})$		✓			
$\Delta\theta_B$		✓			
N_{us}	✓	✓	✓	✓	
$T_{i,us}$		✓			
\mathbf{V}_{us}	✓	✓	✓	✓	
β_{us}		✓			
P_{us}		✓			
θ_{Bn}	✓	✓	✓	✓	✓
$\sigma(\theta_{Bn})$		✓			
\mathbf{n}	✓	✓	✓	✓	✓
M_A	✓	✓	✓	✓	
$\sigma(M_A)$		✓			
M_f		✓			
$\sigma(M_f)$		✓			
M_{ms}					✓
R_{cB}	✓	✓	✓	✓	✓
R_{cn}		✓	✓		
R_{cT}		✓			
position	✓	✓		✓	✓
ΔR	✓	✓			
TQF		✓			
quick-look plots	✓	✓	✓	✓	✓

- standard deviation of θ_{Bn} based on variation in upstream B in the OMNI interval used;
- components n_x , n_y and n_z of the shock normal;
- standard deviation of M_A based on variation in upstream B in the OMNI interval used;
- standard deviation of M_f based on variation in upstream B in the OMNI interval used;
- X_{GSE} , Y_{GSE} and Z_{GSE} coordinates [km] of the spacecraft, when it observed the shock;
- TQF, Tetrahedron quality factor.

Table 1 contains the list of all parameters with marking of which parameters can be available for which missions. The details of parameters for different satellite data are given in the following sections.

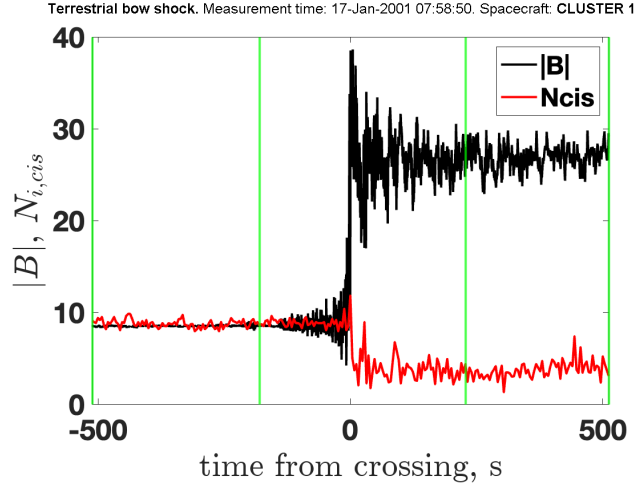


Figure 4: Example of a plot of the terrestrial bow shock, measured by CLUSTER CS1. Shown are the magnetic field magnitude and the ion density.

4.1 Terrestrial shocks

To build a comprehensive catalogue of terrestrial bow shock crossings with their relevant fundamental parameters, the data from Cluster and MMS were used.

The Cluster mission was launched in 2000 and it consists of four identical spacecraft on similar elliptical polar orbits with an initial perigee at about $4 R_E$ ($R_E = 6371$ km is the Earth’s radius) and an apogee at $19.6 R_E$ [Escoubet et al., 2001]. We employed the list of shock crossing observed by Cluster CS1 compiled by Kruparova et al. [2019] for the years of 2001–2013. To obtain the upstream and downstream shock parameters for each crossing, we used the magnetic field data from FGM (Fluxgate Magnetometer) experiment [Balogh et al., 2001] in full resolution, the data from Cluster Ion Spectrometry (CIS) Hot Ion Analyzer (HIA) sensor [Rème et al., 2001] for the ion number densities and flow velocities and the data from the Waves of High frequency and Sounder for Probing of Electron density by Relaxation (WHISPER) sounder [Trotignon et al., 2001] for the electron number densities. Using the obtained parameters, the shock normal \mathbf{n} is identified and the Alfvénic Mach number is calculated. The details of such calculations including the proxy for Mach number based only on parameters obtained from the magnetic field measurements are given by Gedalin et al. [2021]. Figure 4 gives an example of a plot of the terrestrial bow shock as measured by CLUSTER CS1, and available in the SHARP database.

The four-spacecraft MMS mission [Burch et al., 2016] was launched on 12 March 2015 in a 28° equatorial inclination, $12 R_E$ apogee elliptical orbit. Lalti et al. [2022] have compiled the set of 2,797 shock crossings with main shock parameters observed by MMS. The crossings were determined by applying the supervised machine learning technique [Olshevsky et al., 2021]. Measurements of the ion velocity distribution functions (VDF) from Dual Ion Spectrometers (DIS) of the Fast Plasma Investigation (FPI) suite [Pollock et al., 2016] were used to develop a 3D Convolutional Neural Network (CNN). The developed CNN is able to identify the regions which MMS is crossing based only on the ion energy distributions. The shock parameters for the identified shock crossings included ones

related to the spacecraft and data acquisition mode, and the others related to actually shock crossings. The vector normal to the shock \mathbf{n} is calculated using the bow shock model by Farris et al. [1991]. For the main shock parameters (Alfvénic Mach number M_A , fast mode Mach number M_f , the angle between the upstream magnetic field and the shock normal θ_{Bn} , and the upstream plasma beta β_{us}), the time-shifted OMNI database data from spacecraft located upstream of MMS (<https://omniweb.gsfc.nasa.gov/>). In addition, the following parameters are also included: the upstream velocity, density, ion temperature, magnetic field vector, magnetic field magnitude, and the solar wind dynamic pressure for each shock crossing. For compression ratios, the downstream shock parameters are calculated using MMS FPI data. Figure 5 gives an example of a plot of the terrestrial bow shock as measured by MMS 1, and available in the SHARP database.

The mean magnetic field magnitude upstream of the shock is obtained directly from the data for terrestrial shocks using FGM measurements in the full resolution mode onboard MMS and Cluster. For the terrestrial shocks, all vector quantities are in the Geocentric Solar ecliptic (GSE) coordinate system. The SHARP database contains 2797 terrestrial shocks measured by MMS between October 2015 and December 2020, and 472 measured by CLUSTER between January 2001 and December 2012. The shock parameters available in the SHARP shock database for CLUSTER and MMS data are shown in Table 1.

4.2 Interplanetary shocks

The THEMIS mission (Time History of Events and Macroscale Interactions during Substorms) [Angelopoulos, 2008] was launched on February 17, 2007, and employed five identical spacecraft on elliptical, nearly equatorial orbits lined up at apogee every four days. THEMIS was designed to study substorms in the Earth’s magnetosphere. In 2009-2011, two of THEMIS’s probes, B and C, were sent into lunar orbit as part of a new mission under the name ARTEMIS (Acceleration, Reconnection, Turbulence and Electrodynamics of the Moon’s Interaction with the Sun) [Angelopoulos, 2011]. ARTEMIS’s mission is to study the Earth-Moon Lagrange points, the solar wind, the Moon’s plasma wake, and the interaction between Earth’s magnetotail and the Moon’s own weak magnetism. The two spacecraft, orbiting in opposite directions around the Moon, provide the first 3D measurements of the Moon’s magnetic field allowing to determine its regional influence on solar wind particles. Spending more than 70% of orbit time in the solar wind, these satellites provide also a good source of measurements of interplanetary shocks.

The data measured by the spacecraft which are used for the shock analysis include the magnetic field vector, and the velocity vector and density of both ions and electrons. The Fluxgate Magnetometer (FGM) [Auster et al., 2008] measures the ambient magnetic field and its low frequency fluctuations, up to 64 vectors/sec. The Electrostatic Analyzer (ESA) [McFadden et al., 2008] measures the electron and ion distributions in 32 energy channels and 88 angle channels. A full distribution is provided at best at 32 spin cadence, while a reduced distribution is provided at 1 spin cadence. The distributions moments are calculated onboard.

From these, the upstream and downstream values of these parameters were calculated. The Alfvénic Mach number M_A , the shock normal \mathbf{n} and the shock

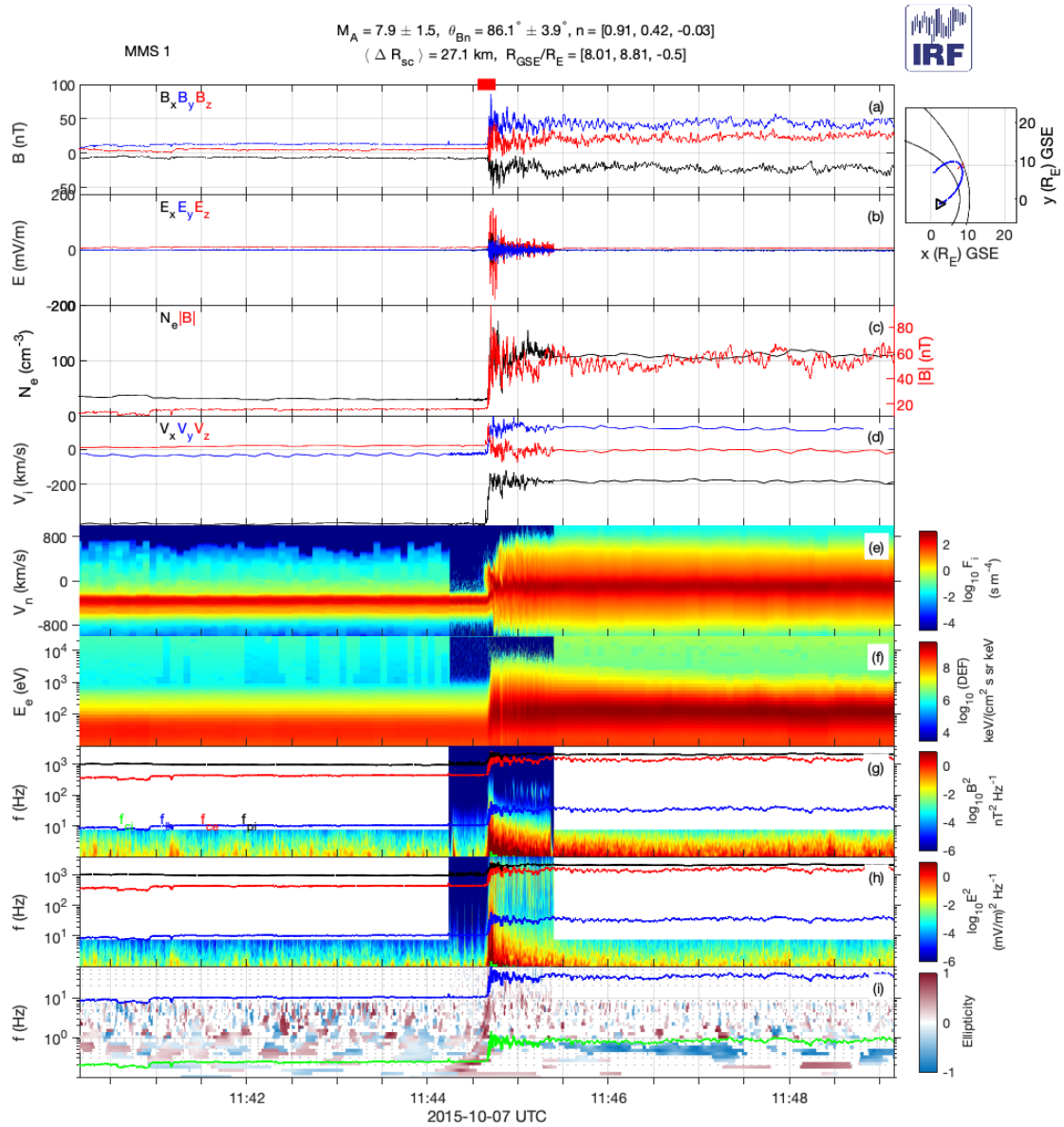


Figure 5: Example of a plot of the terrestrial bow shock, measured by MMS 1. Top to bottom: Magnetic field, electric field, electron density, ion velocity, ion velocity distribution function in the normal direction, electron flux energy spectrum, magnetic field power frequency spectrum, electric field power frequency spectrum, and ellipticity.

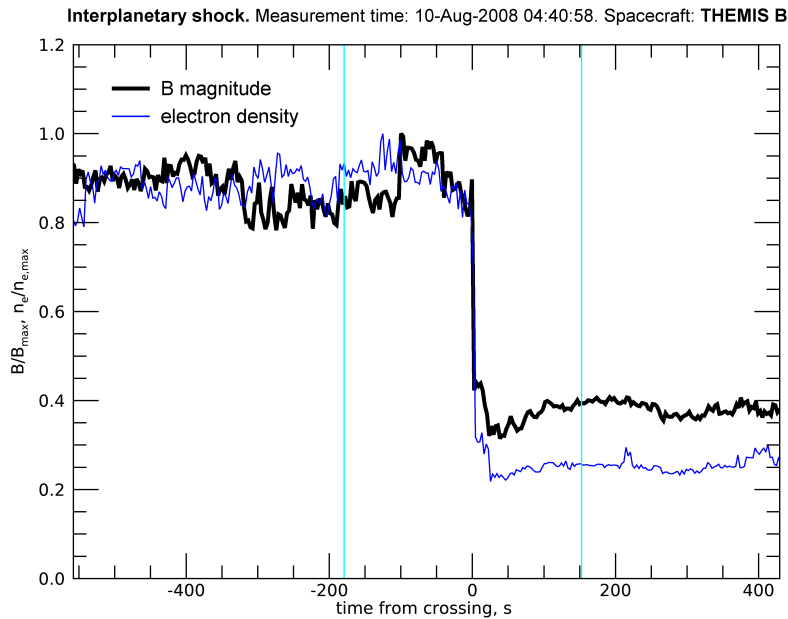


Figure 6: Example of a plot of an interplanetary shock, measured by THEMIS B. Shown are magnetic field magnitude and the electron density, both relative to their maximum value around the shock.

angle θ_{Bn} are calculated using mixed coplanarity. M_A and θ_{Bn} are calculated from magnetic field and electron velocity; \mathbf{n} from magnetic field and ion velocity. The upstream magnetic field and electron density and velocity are stored in the database. All vectors are expressed in the Despun Sun-pointing L-momentum (DSL) coordinate system. Figure 6 gives an example of a plot of an interplanetary shock as measured by THEMIS B, and available in the SHARP database. The SHARP database contains 407 interplanetary shocks measured by THEMIS B and C / ARTEMIS, between June 2008 and November 2019. Table 1 shows the shock parameters available in the SHARP shock database for THEMIS/ARTEMIS data.

4.3 Shocks at non-magnetized planets

Mars and Venus, unlike other planets, do not have global intrinsic magnetic fields. As such, they form a non-magnetised obstacle in the solar wind, and the solar wind magnetic field drapes about the planet, piling up on the dayside, creating an induced magnetosphere. The bow shocks thus formed are much narrower (closer to their planets) than the terrestrial bow shock, and, although not caused by an intrinsic magnetosphere, do involve magnetic effects. These bow shocks as measured by MAVEN (for Mars) and VEX (for Venus) are analysed in the SHARP project. The calculations involved to analyse these shocks in this project have not yet been published elsewhere, and are therefore described in this paper in more detail than those of the other missions.

NASA's Mars Atmosphere and Volatile EvolutioN (MAVEN) mission, launched in 2013, is observing the Martian upper atmosphere [Gruesbeck et al., 2018]. Its goal is to determine the role that loss of atmospheric gas to space played in chang-

ing the Martian climate through time. The Solar Wind Ion Analyser (SWIA) [Halekas et al., 2015] measures the ion distributions at 4s cadence, in the energy range 5 eV to 25 keV, and with a field of view of $360^\circ \times 90^\circ$. The distributions moments, i.e., the velocity vector and ion density of the plasma, assuming all ions are protons, are calculated onboard. The magnetometer MAG [Connerney et al., 2015] measures the ambient magnetic field vector at the intrinsic rate of 32 samples/second. The data, in addition to the spacecraft location, are downloaded from the AMDA Versatile web tool for Space Physics, (<http://amda.cdpp.eu>).

All parameters are given in the Mars Solar Orbital (MSO) coordinate system. In this system, the x -axis points from Mars to the Sun. The y -axis lies in the plane of the Mars-Sun vector and the orbital velocity vector, orthogonal to the x -axis, and quasi-antiparallel to the orbital velocity. The z -axis completes the right-hand system.

The list of MAVEN shock measurement times was obtained from Garnier [2022]. For each of these shocks times, the measured data were analysed over a period of 20 minutes centered around the shock time. The upstream measurement interval was selected as the 2-minute period within the 10-minute upstream side, where the time average of magnetic field magnitude multiplied by ion density is smallest. From this interval, the upstream magnetic field \mathbf{B}_{us} , ion velocity \mathbf{V}_{us} and density N_{us} are calculated as the averages of the respective time-dependent parameters over this interval.

The downstream measurement interval is difficult to select based on any particular parameter-value condition; therefore, this is selected as the period between 6 and 8 minutes downstream of the shock. The downstream plasma parameters \mathbf{B}_{ds} , \mathbf{V}_{ds} and N_{ds} are calculated as averages over this interval.

In order to find the shock normal, a model for the Martian bow shock is used. For this, it is useful to first convert the location data of MAVEN to the aberrated MSO system. With respect to the MSO system, this system is slightly rotated about the z -axis, to account for the relative motion of Mars to the average solar wind direction:

$$\begin{aligned} x_a &= x \cos \psi - y \sin \psi \\ y_a &= x \sin \psi + y \cos \psi \\ z_a &= z \end{aligned} \tag{1}$$

with x , y and z the location of the measurement point of the shock in MSO coordinates, and x_a , y_a and z_a in the aberrated MSO coordinates, and $\psi = 4^\circ$ the aberration (rotation) angle.

The bow shock is modelled as a surface of revolution of a conic section. Hall et al. [2016] and Hall et al. [2019] found that when fitting this model to measurements, the focus location and eccentricity of the shape stayed roughly constant while the semilatus rectum varies. The two former parameters are therefore taken constant, with as values the averages of the values found by Hall et al. [2016] and Hall et al. [2019], which gives the focus location on the x_a -axis $x_0 = 0.75R_M$ (with R_M the radius of Mars) and the eccentricity $\varepsilon = 1.01$ (the latter making the shape very close to a paraboloid). With these, the semilatus rectum L can be calculated from the location of any point at the shock surface, defining the entire shock surface at that point in time. This surface can be characterised by the terminator

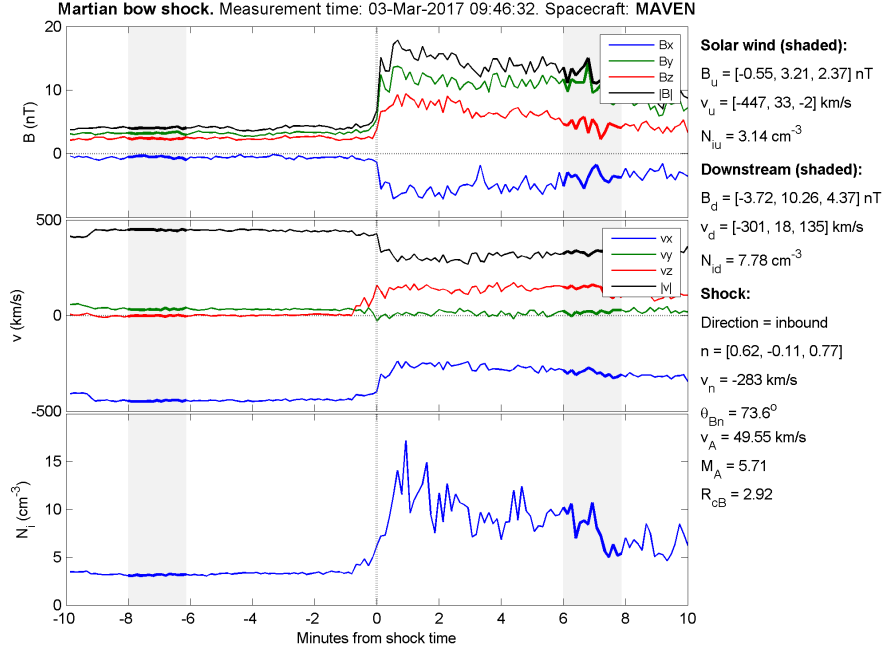


Figure 7: Example of a plot of the Martian bow shock, measured by MAVEN. Upper panel: magnetic field strength. Middle panel: ion velocity. Lower panel: ion density.

distance R_{TD} of the bow shock [Hall et al., 2016], which is given by:

$$R_{TD} = \sqrt{(x_a - x_0)^2 + y_a^2 + z_a^2 + \varepsilon^2 x_a^2 - x_0^2 + 2\varepsilon x_a \sqrt{(x_a - x_0)^2 + y_a^2 + z_a^2}} \quad (2)$$

The shock normal (in the aberrated coordinates) \mathbf{n}_a can then be calculated as:

$$\mathbf{n}_a = [-\sin \alpha, \cos \alpha \cos \phi, \cos \alpha \sin \phi] \quad (3)$$

with:

$$\alpha = \arctan \frac{-\varepsilon \left(\sqrt{x_0^2 + R_{TD}^2} - \varepsilon x_a \right) - x_a + x_0}{\sqrt{\left(\sqrt{x_0^2 + R_{TD}^2} - \varepsilon x_a \right)^2 - (x_a - x_0)^2}} \quad (4)$$

$$\phi = \arctan \frac{z_a}{y_a} \quad (5)$$

The shock normal in non-aberrated MSO coordinates \mathbf{n} is found by applying the inversion of equation (1) to \mathbf{n}_a . Figure 7 gives an example of a plot of the Martian bow shock as measured by MAVEN, and available in the SHARP database.

Venus Express (VEX) [Shan et al., 2015] was ESA's first spacecraft to voyage to Venus; it was built around the design of Mars Express. It studied the planet's complex dynamics and chemistry, and the interactions between the atmosphere and the surface, which provided clues about the surface's characteristics. VEX orbited Venus from 2006 to 2014, providing a sufficiently long duration of observations to give an opportunity to investigate the effects of solar activity on the

Venusian bow shock. VEX had a highly elliptical polar orbit with a periapsis of 250–300 km altitude at 78°N, and crossed the bow shock twice a day. In addition, VEX covered a large range of Solar Zenith Angles (from $\sim 10^\circ$ to $\sim 135^\circ$) at the Venusian bow shock, which is suitable to determine the bow shock locations at both the stand-off and terminator distances.

The magnetometer MAG onboard of VEX consisted of two fluxgate sensors for a separation of magnetic effects of the spacecraft origin from the ambient space magnetic field. The Ion Mass Analyzer (IMA), part of the Analyzer of Space Plasmas and Energetic Atoms (ASPERA-4), measured ion densities and velocities. Both MAG and IMA data were obtained from the AMDA Versatile web tool for Space Physics. The B-field data have a time resolution of 4 seconds. Unfortunately, the ion density and velocity data are available at a low time resolution only (192 seconds).

The observations are presented in the Venus Solar Orbital (VSO) coordinates. In this system, the x -axis points from Venus to the Sun. The y -axis lies in the plane of the Venus-Sun vector and the orbital velocity vector, orthogonal to the x -axis, and quasi-parallel to the orbital velocity. The z -axis completes the right-hand system. Note that this means that the y - and z -axes are oriented opposite to their equivalent in the MSO system.

Two lists of the shocks measured by VEX which were analysed by Shan et al. [2015], one measured during a solar minimum period and one during a solar maximum period, were kindly provided to us by Lu and Shan. For each of these shocks times, the shock normal is determined in a similar way as for the MAVEN data. The location data of VEX are converted to an aberrated VSO coordinate system to correct for the solar wind direction relative to the planet's motion (see Eq. (1)), with $\psi = -4.7^\circ$. The bow shock model is similar to the Martian one, i.e. a surface of revolution of a conic section, where the focus location and eccentricity stay relatively constant while the semilatus rectum varies with time. Shan et al. [2015] found from the VEX data $x_0 = 0.596R_V$ (R_V being the radius of Venus) and $\varepsilon = 1.03$ during solar minimum, and $x_0 = 0.775R_V$ and $\varepsilon = 1.096$ during solar maximum; these values are also used for the respective subsets of the shock list here. The shock normal \mathbf{n} at each measurement is determined following the same steps as in the case of Mars; see above.

For each shock, the measured data are analysed over a period of 20 minutes centered around the shock time. The length of averaging periods for the up- and downstream B-field values is this time chosen as 192 seconds, to match the time resolution of the \mathbf{V} and N measurements. The upstream measurement interval is selected as the 192s period within the 10-minute upstream side, where the time average of magnetic field magnitude $|\mathbf{B}|$ is smallest. From this interval, the upstream magnetic field vector \mathbf{B}_{us} is calculated as the average of the time-dependent magnetic field vector. The upstream ion velocity vector \mathbf{V}_{us} and density N_{us} are taken as the sample values from the time series data whose time stamp falls within this 3.2 minute period.

Because the ion velocity and density from VEX are available from AMDA at such low time resolution, these data are not suitable to be used for the Alfvén velocity. Therefore, another method to determine a Mach number for these shocks must be used. Following Zhang et al. [2008], the magnetosonic Mach number M_{ms} is determined from the shock strength and θ_{Bn} , assuming the plasma is isotropic

and Maxwellian both upstream and downstream. In this situation, the Rankine-Hugoniot condition is formulated as given by Kivelson and Russell [1995] (equation (3.86) in their book):

$$\frac{1}{2} + \frac{\beta\gamma}{2M_{ms}^2(\gamma-1)} + \frac{\sin^2\theta_{Bn}}{M_{ms}^2} = \frac{1}{2R_{cN}^2} + \frac{u^2}{2} + \frac{R_{cBz}\sin^2\theta_{Bn}}{M_{ms}^2} + \frac{\gamma}{R_{cN}(\gamma-1)} \left[1 - \frac{1}{R_{cN}} + \frac{\beta}{2M_{ms}^2} - \frac{(R_{cBz}^2-1)\sin^2\theta_{Bn}}{2M_{ms}^2} \right] \quad (6)$$

with

$$u = \frac{\sin\theta_{Bn}\cos\theta_{Bn}(R_{cN}-1)}{M_{ms}^2 - R_{cN}\cos^2\theta_{Bn}} \quad (7)$$

the plasma density compression ratio R_{cN} is given by

$$R_{cN} = \frac{R_{cBz}M_{ms}^2}{M_{ms}^2 + \cos^2\theta_{Bn}(R_{cBz}-1)} \quad (8)$$

and R_{cBz} is the compression ratio of the magnetic field parallel to the shock front. β is assumed 1, and the ratio of specific heats γ of the plasma as 5/3. Eq. (6) is numerically inverted to calculate M_{ms} from R_{cBz} and θ_{Bn} .

An assumption for the Rankine-Hugoniot relation is also that the normal component of the B field is not modified by the shock. Because of this, the downstream period is chosen as the 192-second period (within the analysed 10-minute downstream side) where the averaged value of $\mathbf{B} \cdot \mathbf{n}$ (i.e. normal component of B field) is closest to $\mathbf{B}_{us} \cdot \mathbf{n}$. From this interval, the downstream magnetic field vector \mathbf{B}_{ds} is calculated as the average of the time-dependent magnetic field vector. Consequently R_{cBz} is found from:

$$R_{cBz} = \frac{|\mathbf{B}_{us} - (\mathbf{B}_{us} \cdot \mathbf{n})\mathbf{n}|}{|\mathbf{B}_{ds} - (\mathbf{B}_{ds} \cdot \mathbf{n})\mathbf{n}|} \quad (9)$$

The downstream ion velocity vector \mathbf{V}_{ds} and density N_{ds} are taken as the sample values from the time series data whose time stamp falls within the same downstream 192-s period.

Figure 8 gives an example of a plot of the Venusian bow shock as measured by VEX, and available in the SHARP database.

The SHARP database contains 1660 Martian bow measurements by MAVEN between November 2014 and April 2017, and 776 Venusian bow shock measurements by VEX, measured between August 2008 and May 2009 (solar minimum) and between May 2011 and February 2012 (solar maximum). Table 1 lists the parameters available for MAVEN and VEX data.

5 References

- V. Angelopoulos. The THEMIS mission. *Space Sci. Rev.*, 141(1–4):5–34, 2008. doi: doi.org/10.1007/s11214-008-9336-1.

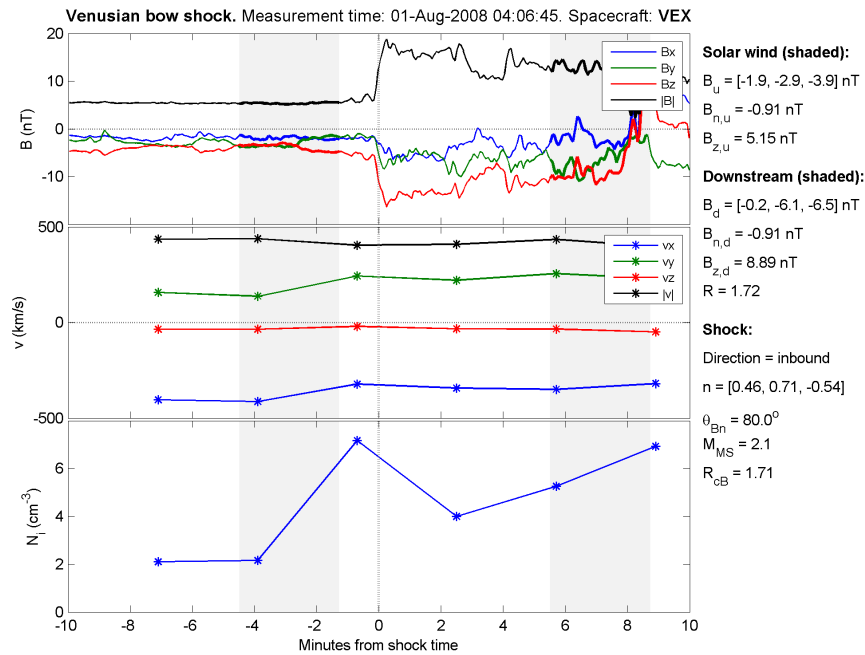


Figure 8: Example of a plot of the Venusian bow shock, measured by VEX. Upper panel: magnetic field strength. Middle panel: ion velocity. Lower panel: ion density.

V. Angelopoulos. The ARTEMIS mission. *Space Sci. Rev.*, 165(1–4):3–25, 2011. doi: doi.org/10.1007/s11214-010-9687-2.

H. U. Auster, K. H. Glassmeier, W. Magnes, O. Aydogar, W. Baumjohann, D. Constantinescu, D. Fischer, K. H. Fornacon, E. Georgescu, P. Harvey, O. Hillenmaier, R. Kroth, M. Ludlam, Y. Narita, R. Nakamura, K. Okrafka, F. Plaschke, I. Richter, H. Schwarzl, B. Stoll, A. Valavanoglou, and M. Wiedemann. The THEMIS Fluxgate Magnetometer. *Space Science Reviews*, 141: 235–264, 2008. ISSN 1572-9672. doi: 10.1007/s11214-008-9365-9.

A. Balogh, C. M. Carr, M. H. Acuña, M. W. Dunlop, T. J. Beek, P. Brown, K.-H. Fornacon, E. Georgescu, K.-H. Glassmeier, J. Harris, G. Musmann, T. Oddy, and K. Schwingenschuh. The cluster magnetic field investigation: overview of in-flight performance and initial results. *Annales Geophysicae*, 19(10/12):1207–1217, 2001. doi: 10.5194/angeo-19-1207-2001.

J. L. Burch, T. E. Moore, R. B. Torbert, and B. L. Giles. Magnetospheric multiscale overview and science objectives. *Space Sci. Rev.*, 199(1–4):5–21, 2016. doi: 10.1007/s11214-015-0164-9.

J. E. P. Connerney, J. Espley, P. Lawton, S. Murphy, J. Odom, R. Oliverson, and D. Sheppard. The MAVEN Magnetic Field Investigation. *Space Science Reviews*, 195:257–291, 2015. doi: 10.1007/s11214-015-0169-4.

C. P. Escoubet, M. Fehringer, and M. Goldstein. Introduction the cluster mission. *Annales Geophysicae*, 19(10/12):1197–1200, 2001. doi: 10.5194/angeo-19-1197-2001.

- M. H. Farris, S. M. Petrinec, and C. T. Russell. The thickness of the magnetosheath: Constraints on the polytropic index. *Geophysical Research Letters*, 18(10):1821–1824, 1991. doi: <https://doi.org/10.1029/91GL02090>.
- Garnier. Martian shock crossings dataset, 2022. V. 0.1.
- M. Gedalin, C. T. Russell, and Dimmock. Shock mach number estimates using incomplete measurements. *Journal of Geophysical Research: Space Physics*, 126:e2021JA029519, 2021. doi: doi.org/10.1029/2021JA029519.
- J. R. Gruesbeck, J. R. Espley, J. E. P. Connerney, G. A. DiBraccio, Y. I. Soobiah, D. Brain, C. Mazelle, J. Dann, J. Halekas, and D. L. Mitchell. The three-dimensional bow shock of mars as observed by maven. *Journal of Geophysical Research: Space Physics*, 123:4542–4555, 2018. doi: [10.1029/2018JA025366](https://doi.org/10.1029/2018JA025366).
- J. S. Halekas, E. R. Taylor, G. Dalton, G. Johnson, D. W. Curtis, J. P. McFadden, D. L. Mitchell, R. P. Lin, and B. M. Jakosky. The Solar Wind Ion Analyzer for MAVEN. *Space Science Reviews*, 195:125–151, 2015. doi: [10.1007/s11214-013-0029-z](https://doi.org/10.1007/s11214-013-0029-z).
- B. E. S. Hall, M. Lester, B. Sánchez-Cano, J. D. Nichols, D. J. Andrews, N. J. T. Edberg, H. J. Opgenoorth, M. Fränz, M. Holmström, R. Ramstad, O. Witasse, M. Cartacci, A. Cicchetti, R. Noschese, and R. Orosei. Annual variations in the Martian bow shock location as observed by the Mars Express mission. *J. Geophys. Res. Space Physics*, 121:11,474–11,494, 2016. doi: [10.1002/2016JA023316](https://doi.org/10.1002/2016JA023316).
- B. E. S. Hall, B. Sánchez-Cano, J. A. Wild, M. Lester, and M. Holmström. The Martian bow shock over solar cycle 23–24 as observed by the Mars Express mission. *Journal of Geophysical Research: Space Physics*, 124:4761–4772, 2019. doi: [10.1029/2018JA026404](https://doi.org/10.1029/2018JA026404).
- M. G. Kivelson and C. T. Russell. *Introduction to Space Physics*. Cambridge Univ. Press, Cambridge, U. K., 1995.
- O. Kruparova, V. Krupar, J. Šafránková, Z. Němeček, M. Maksimovic, O. Santolik, J. Soucek, F. Němec, and J. Merka. Statistical survey of the terrestrial bow shock observed by the cluster spacecraft. *Journal of Geophysical Research: Space Physics*, 124(3):1539–1547, 2019. doi: <https://doi.org/10.1029/2018JA026272>.
- A. Lalti, Yu. V. Khotyaintsev, A. P. Dimmock, A. Johlander, D. B. Graham, and V. Olshevsky. A database of mms bow shock crossings compiled using machine learning. *Journal of Geophysical Research: Space Physics*, 127(8):e2022JA030454, 2022. doi: <https://doi.org/10.1029/2022JA030454>.
- J P McFadden, C W Carlson, D Larson, M Ludlam, R Abiad, B Elliott, P Turin, M Marckwordt, and V Angelopoulos. The THEMIS ESA Plasma Instrument and In-flight Calibration. *Space Science Reviews*, 141:277–302, 2008. doi: [10.1007/s11214-008-9440-2](https://doi.org/10.1007/s11214-008-9440-2).
- V. Olshevsky, Y. V. Khotyaintsev, A. Lalti, A. Divin, G. L. Delzanno, and S. et al. Anderzén. Automated classification of plasma regions using 3d particle energy distributions. *Journal of Geophysical Research: Space Physics*, 126(10):e2021JA029620, 2021. doi: doi.org/10.1029/2021ja029620.

- C. Pollock, T. Moore, A. Jacques, J. Burch, U. Gliese, Y. Saito, T. Omoto, L. Avanov, A. Barrie, V. Coffey, J. Dorelli, D. Gershman, B. Giles, T. Rosnack, C. Salo, S. Yokota, M. Adrian, C. Aoustin, C. Auletta, S. Aung, V. Bigio, N. Cao, M. Chandler, D. Chornay, K. Christian, G. Clark, G. Collinson, T. Corris, A. De Los Santos, R. Devlin, T. Diaz, T. Dickerson, C. Dickson, A. Diekmann, F. Diggs, C. Duncan, A. Figueroa-Vinas, C. Firman, M. Freeman, N. Galassi, K. Garcia, G. Goodhart, D. Guererro, J. Hageman, J. Hanley, E. Hemminger, M. Holland, M. Hutchins, T. James, W. Jones, S. Kreisler, J. Kujawski, V. Lavu, J. Lobell, E. LeCompte, A. Lukemire, E. MacDonald, A. Mariano, T. Mukai, K. Narayanan, Q. Nguyen, M. Onizuka, W. Paterson, S. Persyn, B. Pieprgrass, F. Cheney, A. Rager, T. Raghuram, A. Ramil, L. Reichenthal, H. Rodriguez, J. Rouzaud, A. Rucker, Y. Saito, M. Samara, J. A. Sauvaud, D. Schuster, M. Shappirio, K. Shelton, D. Sher, D. Smith, K. Smith, S. Smith, D. Steinfeld, R. Szymkiewicz, K. Tanimoto, J. Taylor, C. Tucker, K. Tull, A. Uhl, J. Vloet, P. Walpole, S. Weidner, D. White, G. Winkert, P.-S. Yeh, and M. Zeuch. Fast Plasma Investigation for Magnetospheric Multiscale. *Space Sci. Rev.*, 199(1–4):331–406, 2016. doi: doi.org/10.1007/s11214-016-0245-4.
- H. Rème, C. Aoustin, J. M. Bosqued, I. Dandouras, B. Lavraud, J. A. Sauvaud, A. Barthe, J. Bouyssou, Th. Camus, O. Coeur-Joly, A. Cros, J. Cuvilo, F. Ducay, Y. Garbarowitz, J. L. Medale, E. Penou, H. Perrier, D. Romefort, J. Rouzaud, C. Vallat, D. Alcaydé, C. Jacquy, C. Mazelle, C. d’Uston, E. Möbius, L. M. Kistler, K. Crocker, M. Granoff, C. Mouikis, M. Popecki, M. Vosbury, B. Klecker, D. Hovestadt, H. Kucharek, E. Kueneth, G. Paschmann, M. Scholer, N. Sckopke, E. Seidenschwang, C. W. Carlson, D. W. Curtis, C. Ingraham, R. P. Lin, J. P. McFadden, G. K. Parks, T. Phan, V. Formisano, E. Amata, M. B. Bavassano-Cattaneo, P. Baldetti, R. Bruno, G. Chionchio, A. Di Lellis, M. F. Marcucci, G. Pallocchia, A. Korth, P. W. Daly, B. Graeve, H. Rosenbauer, V. Vasyliunas, M. McCarthy, M. Wilber, L. Eliasson, R. Lundin, S. Olsen, E. G. Shelley, S. Fuselier, A. G. Ghielmetti, W. Lennartsson, C. P. Escoubet, H. Balsiger, R. Friedel, J.-B. Cao, R. A. Kovrazhkin, I. Papamastorakis, R. Pellat, J. Scudder, and B. Sonnerup. First multispacecraft ion measurements in and near the earth’s magnetosphere with the identical cluster ion spectrometry (cis) experiment. *Annales Geophysicae*, 19(10/12):1303–1354, 2001. doi: 10.5194/angeo-19-1303-2001.
- Lican Shan, Quanming Lu, Christian Mazelle, Can Huang, Tielong Zhang, Mingyu Wu, Xinliang Gao, and Shui Wang. The shape of the Venusian bow shock at solar minimum and maximum: Revisit based on VEX observations. *Planetary and Space Science*, 109-110:32–37, 2015. doi: 10.1016/j.pss.2015.01.004.
- J. G. Trotignon, P. M. E. Décréau, J. L. Rauch, O. Randriamboarison, V. Krasnoselskikh, and P. et al. Canu. How to determine the thermal electron density and the magnetic field strength from the cluster/whisper observations around the earth. *Annales Geophysicae*, 19(10/12):1711–1720, 2001. doi: 10.5194/angeo-19-1711-2001.
- T. L. Zhang, S. Pope, M. Balikhin, C. T. Russell, L. K. Jian, M. Volwerk, M. Delva, W. Baumjohann, C. Wang, J. B. Cao, M. Gedalin, K.-H. Glassmeier, and

K. Kudela. Venus Express observations of an atypically distant bow shock during the passage of an interplanetary coronal mass ejection. *J. Geophys. Res.*, 113(E00B12), 2008. doi: 10.1029/2008JE003128.